THE JOURNAL OF PHYSICAL CHEMISTRY C

ARTICLE

pubs.acs.org/JPCC

Self-Assembled Poly(ethylene glycol) Buffer Layers in Polymer Solar Cells: Toward Superior Stability and Efficiency

Shang-Chieh Chien,[†] Fang-Chung Chen,[*,‡] Ming-Kai Chung,[†] and Chain-Shu Hsu[§]

[†]Department of Photonics and Institute of Electro-optical Engineering, [‡]Department of Photonics and Display Institute, and [§]Department of Applied Chemistry, National Chiao Tung University, Hsinchu 30010, Taiwan

Supporting Information

ABSTRACT: In this study, we have systematically investigated the mechanism behind the formation of nanoscale self-assembled polymer buffer layers at the cathode interfaces of polymer solar cells. Poly(ethylene glycol) (PEG) molecules in a polymer blend, comprising poly(3-hexylthiophene) and [6,6]-phenyl-C_{61}-butyric acid methyl ester, spontaneously migrated to the surface where they reacted with the Al cathode to form ohmic contacts. In terms of thermodynamics, the surface energy of the substrates played an important role in triggering the vertical-type morphology. From a kinetics point of view, PEG polymers having lower molecular weights readily underwent vertical phase separation prior to solidification of the polymer films, due to their higher mobilities, whereas PEG polymers of higher molecular weights tended to become trapped in the active layer. Employing this knowledge, we prepared organic photovoltaic cells exhibiting both high efficiency and appreciable improvement in stability.

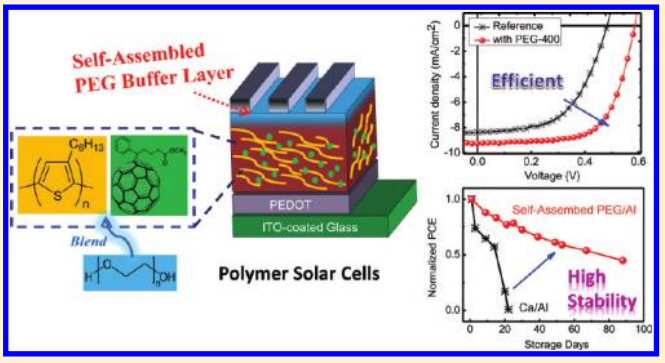

INTRODUCTION

The rising awareness of global environmental issues and a foreboding energy crisis has led to widespread recognition of the need for renewable energy technologies,[1,2] with photovoltaic technology being considered as one of the most promising methods for directly harnessing solar energy. Among the various kinds of photovoltaic devices, organic photovoltaic cells (OPVs) based on polymer materials are particularly interesting systems for harvesting solar energy[3−5] because of their light weight, mechanical flexibility, and ability to prepare large-area solar panels at low cost.[6−8] Furthermore, low-temperature processing would certainly save energy during their mass production, thereby shortening the energy payback time—a critical figure-of-merit when evaluating a photovoltaic technology.[9,10]

Upon the absorption of photons in organic materials, tightly bound electron/hole pairs—excitons—are generated.[11,12] To obtain a high photocurrent, large-area electron donor−acceptor (p−n) interfaces are required to dissociate the excitons into free charges. The bulk heterojunction configuration, comprising conjugated polymers and C_{60} derivatives, is classified currently as the most efficient approach for achieving highly concentrated p−n interfaces to facilitate charge separation.[13] Many techniques, including annealing treatment,[14,15] controlling the surface energy of the substrates,[16] and the use of cosolvent systems,[12,17] have been employed in the quest for the optimized morphology of this blended system and to further improve device efficiency. With more recently developed low-band-gap materials, high power conversion efficiencies (PCEs) of 6−9% have been demonstrated.[18−21]

Interfacial engineering of OPVs—that is, of the interfaces between the photoactive layer and electrodes—is another important approach toward improving device efficiency and stability.[22−24] Ohmic contacts at both the anode and cathode are required to achieve a high charge collection efficiency; the nature of these contacts also determines the open-circuit voltage (V_{oc}).[25,26] At the anodic interface, the conducting polymer poly(3,4-(ethylenedioxy)thiophene):poly(styrenesulfonate) (PEDOT:PSS) is commonly used as the buffer layer (BL) to decrease the barrier height between the photoactive layer and the indium tin oxide (ITO) electrode; solution-processable graphene oxide (GO)[27] and molecule-based monolayers[28] are other potential alternatives. Alkali-metal complexes (LiF,[29] CsF,[30] Cs_2CO_3[31]), water-soluble polyfluorene (PFO) derivatives,[32] and poly(ethylene oxide) (PEO)[33] are all effective cathode BLs for high-performance OPVs. Nevertheless, one additional fabrication step, which complicates the device fabrication processes and increases the cost, is required when using these functional BLs. Furthermore, because the cathode is usually more sensitive to oxygen and moisture in the atmosphere, the environmental stability of these BLs becomes another important concern;[34] many of the reported cathode BLs suffer from long-term operational instability.

Recently, we demonstrated a simple approach—through spontaneous vertical phase separation—for the formation of a cathode BL in polymer solar cells.[35] As illustrated in Figure 1,

Received: November 17, 2011
Revised: November 25, 2011
Published: December 01, 2011

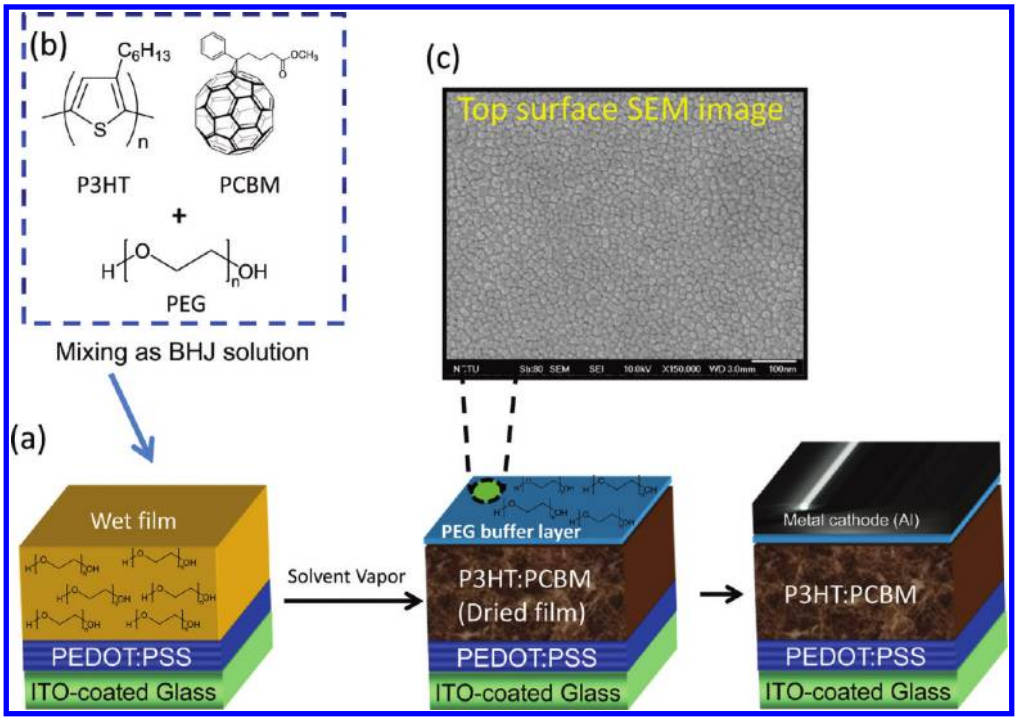

Figure 1. (a) Schematic representation of the formation of a nanoscale PEG BL through spontaneous vertical phase separation in a polymer solar cell. (b) Chemical structures of the materials (P3HT, PCBM, PEG) used in this study. (c) SEM image of the top surface of the P3HT:PCBM:PEG-400 thin film.

we spin-coated solutions comprising poly(3-hexylthiophene) (P3HT), [6,6]-phenyl-C_{61}-butyric acid methyl ester (PCBM), and small amounts of poly(ethylene glycol) (PEG) onto a PEDOT:PSS-coated indium tin oxide (ITO) substrate. During the solvent evaporation process, the PEG molecules migrated vertically to the active layer's surface to naturally form a nanoscale BL, the morphology of which was verified using scanning electron microscopy (SEM; Figure 1).[35] After thermal deposition of the Al electrode, chemical interactions between the self-organized PEG layer and the Al atoms resulted in an effective ohmic contact at the cathode interface, thereby improving the device efficiency.[36] More importantly, the resulting devices incorporating PEG molecules exhibited not only high PCEs but also comparatively superior device stability, presumably due to the thermodynamically stable interface.[35]

More recently, several other functional molecules incorporating PEG-like moieties have displayed similar vertical phase separation.[37,38] For example, Jung et al. reported the improved efficiency and stability of OPVs after blending a fullerene-end-capped PEG derivative (PEG−C_{60}), which self-segregated to the surface of the photoactive film, forming an ideal vertical morphology.[38] We became interested in investigating the mechanism underlying the vertical phase separation process. In this study, we found that the surface energy of the substrates plays an important role in triggering the vertical-type morphology. Furthermore, we also systematically investigated the effect of the PEG molecular weight (M_w) on the device performance, finding PEG polymers with lower values of M_w readily underwent vertical phase separation to improve the device performance, whereas those with higher values tended to become trapped in the active layer. Finally, on the basis of our understanding of the mechanism behind vertical phase separation, we developed OPVs exhibiting both high efficiency and extreme stability.

EXPERIMENTAL METHODS

The device structure used in this study is illustrated in Figure 1. The ITO substrates were routinely cleaned through sonication in detergent, followed by sequential washing in deionized water, acetone, and 2-propanol. The glass ITO substrates were then dried in an oven overnight. Prior to use, the ITO surface was further treated with UV-ozone. PEDOT:PSS (Baytron 4071) was deposited on these substrates at a thickness of 45 nm, and then the resulting thin films were baked at 120 °C for 1 h. The photoactive layer comprised P3HT (Rieke Metals) and PCBM (Solenne) at a weight ratio of 1:1. The photoactive film was spin-coated in a N_2-filled glovebox from a solution of 1,2-dichlorobenzene. For the devices containing PEG, PEG polymers of various molecular weights were blended into the P3HT:PCBM solutions. After spin-coating, the wet films were subjected to a solvent annealing process.[14,39] Finally, a 100 nm thick layer of Al was deposited at a rate of 0.5 nm s^{-1} through thermal evaporation at a pressure of ca. 5×10^{-6} Torr.

Current density−voltage ($J-V$) curves were recorded using the Keithley 2400 source measure system; the photocurrent densities were obtained while the OPVs were illuminated with a 150 W Thermal Oriel solar simulator (AM1.5G). The light intensity was calibrated employing a standard Si photodiode detector equipped with a KG-5 filter (Hamamatsu, Inc.).[40] SEM images were obtained using a JEOL (Tokyo Japan) JSM-7041 field emission scanning electron microscope equipped with an Oxford INCA energy 350 system and operated at electron accelerating voltages ranging from 0.1 to 30 kV. The ultraviolet photoelectron spectrometer used to measure the work functions of the thin films employed 50 W vacuum ultraviolet (VUV) light to excite the valence electrons and secondary electrons; the beam diameter was 1.7 mm, and the incident angle was fixed at 45°.

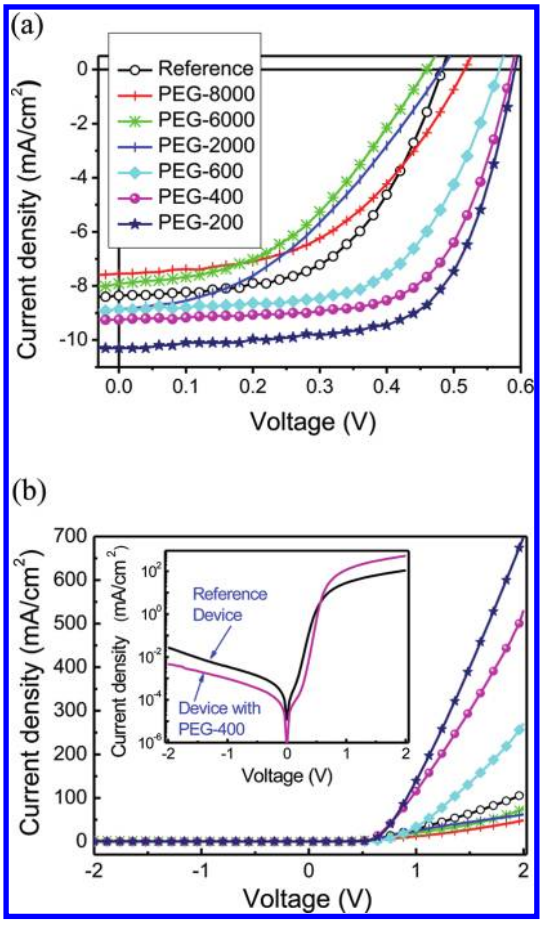

Figure 2. Current density−voltage (J−V) curves of devices prepared with PEG polymers of various molecular weights, measured (a) under illumination and (b) in the dark. Inset in (b): J−V curves (log scale) measured in the dark for devices prepared without (reference device) and with PEG-400.

A PHI 5000 VersaProbe scanning electron spectroscopy for chemical analysis (ESCA) microprobe system (ULVAC-PHI, Chigasaki, Japan) equipped with a windowless He discharge light source (HIS 13 VUV source, Focus GmbH, Taunusstein, Germany) provided He(I) emission at 21.2 eV. To ensure the collection of low-energy electrons, the samples were biased at −5 V. The energy axis of the spectra was calibrated by detecting the secondary electron cutoff.[41]

RESULTS AND DISCUSSION

To investigate the effect of the molecular weight, we blended PEG polymers having values of M_w ranging from 200 to 8000 with the photoactive layer in the photovoltaic devices. Herein, we denote these PEG polymers in the form "PEG-M_w value"; for example, PEG-200 represents the PEG polymer having a molecular weight of 200. Figure 2a displays representative current density−voltage (J−V) curves, recorded under illumination at 100 mW cm^{-2} (AM 1.5G), for devices incorporating PEG polymers of various molecular weights; note that the weight concentration of PEG was optimized for each value of M_w. The reference device, in which no PEG was blended and only Al was used as the cathode, exhibited typical device performance, comparable with those of devices prepared without any cathode BL.[31,32] The open-circuit voltage (V_{oc}), short-circuit current density (J_{sc}), and fill factor (FF) were 0.49 V, 8.36 mA cm^{-2}, and 54%, respectively, giving a PCE of 2.3%. The device performance improved significantly when the photoactive layer contained low-M_w PEG polymers (PEG-200, -400, and -600). For example, for the device containing PEG-200, the values of J_{sc}, V_{oc}, and FF increased significantly to 10.32 mA cm^{-2}, 0.59 V, and 66%, respectively, resulting in a PCE of 4.0%. Table 1 lists the detailed device parameters for each of the OPVs. The device series resistance (R_s), calculated from the J−V curves measured in the dark, decreased dramatically from 12.51 to ca. 1.5 Ω/cm^2 after the addition of PEG-200 to the photoactive layer (Table 1). Because PEG itself is not conducting, this lower value of R_s presumably arose from the decreased contact resistance. We infer that the chemical interactions between the PEG polymers and Al atoms effectively lowered the barrier height, thereby decreasing the device contact resistance.[36] In contrast, the devices fabricated with high-M_w PEG polymers (PEG-2000, -6000, and -8000) exhibited inferior device performance relative to the unmodified device (Figure 2a), even though the values of V_{oc} remained almost unchanged.

The SEM image in Figure S1 (Supporting Information) reveals that the surface of the polymer blend containing PEG-6000 was very smooth, indicating that a PEG BL probably did not form on the polymer blend. In this case, the insulating properties of high-M_w PEG in the polymer blend presumably increased the bulk resistance, leading to an increased value of R_s and a lower PCE. Notably, the optimized weight concentrations of the high-M_w PEGs were less than those in the devices containing the lower M_w counterparts. We suspect that high-M_w PEG polymers were more likely to become entangled with the P3HT polymer chains, thereby inhibiting their vertical phase separation to the top of the active layer. On the other hand, the higher mobility of the low-M_w PEGs in the polymer films allowed their effective migration to the surface of the photoactive films during the drying of the polymer blends. Furthermore, a high concentration of PEG-200 (up to 30%) could be incorporated into the active layer of the device, suggesting that vertical phase separation could proceed more readily in the case of PEG polymers of lower molecular weight.

To further investigate the diode characteristics, we measured the J−V characteristics of these devices in the dark (Figure 2b). Compared with the reference device, the devices prepared with low-M_w PEGs featured higher current densities under forward-bias conditions, indicating that the addition of PEG could promote electron injection from the cathode. In contrast, the addition of higher M_w PEG decreased the current density dramatically, consistent with our hypothesis regarding polymer mobility. The presence of the insulating PEG molecules inevitably increased the device resistance. Furthermore, the inset in Figure 2b presents the log-scale J−V curves of the reference cell and the device incorporating PEG-400; the blending of PEG-400 in the active layer decreased the dark current in both the reverse- and forward-bias regions, suggesting that the self-organized PEG BL could also help to block the leakage current because of its wide band gap.[42] Therefore, the device's rectification ratio (at ±2 V), which is related to the diode characteristics, increased significantly from 4.0 × 10^3 to 1.2 × 10^5 after incorporation of PEG-400 into the photoactive layer.

In Table 1, we observe larger values of V_{oc} for the devices prepared with PEG. Because the open-circuit voltage is sensitive to the contacts at both electrodes, we suspected that the work function of the cathode was modified after the formation of the

self-organized BL. To test this hypothesis, we used ultraviolet photoelectron spectroscopy (UPS) to probe the work functions of Al deposited on active layers prepared with and without PEG-400 (Figure 3). The reference cell was the sample fabricated without PEG. Because we expected the chemical reactions between the Al atoms and PEG polymers to occur only at the surface of the thin films, we deposited 5 nm thick Al onto both types of P3HT:PCBM thin films. The cutoff binding energy shifted significantly to higher value (by 2.3 eV) for the thin film blended with PEG-400, relative to that of the unmodified blend. The UPS data strongly suggest that the work function of the modified cathode was altered to improve the electron injection; that is, effective contact was formed at the cathode interface. Therefore, the UPS data confirmed that blending PEG into the active layer can indeed lower the contact resistance of the cathode interface. Furthermore, we observed a higher open-circuit voltage as a result of the increased built-in potential across the active layer.[31,33,43]

Table 1. Electrical Characteristics of Devices Fabricated with PEG Polymers of Various Molecular Weights

device condition (concn, wt %[a])	V_{oc} (V)	J_{sc} (mA cm^{-2})	FF (%)	PCE (%)	R_s (Ω cm^{-2})[b]
reference device (without PEG)	0.49	8.36	54	2.3	12.5
PEG-200 (30)	0.59	10.32	66	4.0	1.5
PEG-400 (10)	0.59	9.25	65	3.6	2.7
PEG-600 (5)	0.57	8.87	60	3.0	7.0
PEG-2000 (5)	0.49	8.88	40	1.7	20.5
PEG-6000 (5)	0.45	7.92	45	1.6	22.8
PEG-8000 (5)	0.51	7.55	49	1.9	30.8

[a] Optimized PEG weight percentage relative to P3HT. [b] The series resistance was calculated from the log scale $J-V$ curves recorded in the dark.

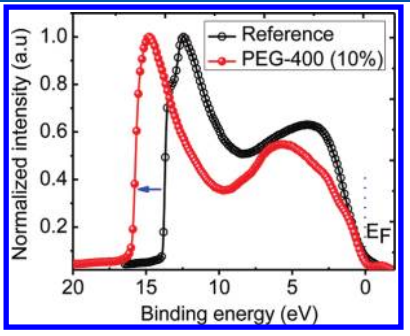

Figure 3. UPS spectra of P3HT:PCBM thin films before and after the addition of PEG-400. A 5 nm thick layer of Al metal was deposited above the polymer thin films through thermal evaporation.

The surface energy of the substrate can affect the morphology of a polymer blend significantly; indeed, controlling the surface energy of the substrate is an effective approach toward achieving OPVs with optimized morphologies.[16,44] For example, Björstrom et al. investigated the distribution of the conjugated polymer and fullerene in polymer blends, obtaining direct evidence that the surface energy determined the morphology of the spin-coated films.[45] More recently, we found that the distribution of PEG polymers in P3HT:PCBM films could be altered through modification of the substrate surface.[46] To explore the substrate effect, we used another hole-collection material, molybdenum trioxide (MoO_3), to modify the surface energy. Using the Zisman method,[47] we calculated the surface energies of PEDOT:PSS and MoO_3 to be 77.8 and 362.2 mN m^{-1}, respectively. Figure 4 displays the devices' $J-V$ characteristics; Table S1 (Supporting Information) summarizes their electrical parameters. The performance of the device prepared with MoO_3 degraded significantly after PEG-400 was blended into the active layer (Figure 4b); its value of V_{oc} decreased from 0.45 to 0.15 V, suggesting that the PEG strands could not migrate to the surface. The insulating properties of PEG only increased the series resistance of the device when the PEG polymer strands remained in the bulk of the active layer.

Figure 5 displays SEM images of P3HT:PCBM films spin-coated onto the PEDOT:PSS and MoO_3 substrates. The films prepared without PEG on both surfaces exhibited very smooth morphologies (Figure 5a,b), whereas the thin film containing PEG-400 deposited on the PEDOT:PSS surface displayed many dotlike nanoscale features (Figure 5c). This finding is consistent with our previous report, in which we inferred the "dotlike" phase to contain PEG molecules.[35] In contrast, no apparent dotlike phase appeared after we deposited the film containing PEG-400 onto the MoO_3-modified substrate (Figure 5d), confirming that most of the PEG molecules remained in the bulk of this P3HT:PCBM blend.

To further examine the substrate effect, we prepared polymer thin film samples, containing 10% PEG-400, on both PEDOT:PSS and MoO_3 surfaces and then immersed them into a water bath. Interestingly, the two samples displayed entirely different behavior (Figure 6). The thin film deposited on the PEDOT:PSS surface remained tightly bonded to the substrate after being placed in the water bath; we infer that all of the blended PEG molecules moved to the surface without influencing the hydrophobic nature of the P3HT:PCBM film, even though the PEG

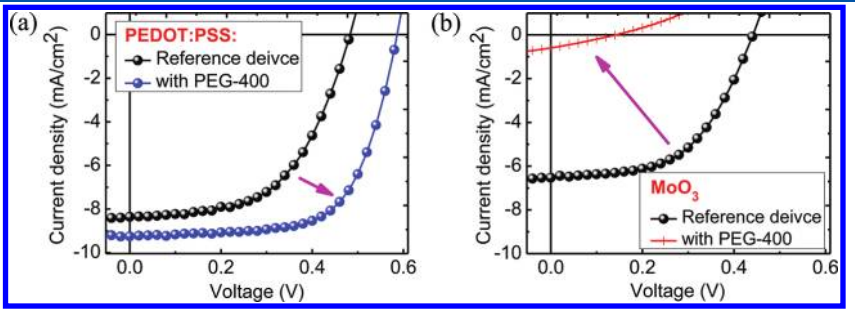

Figure 4. $J-V$ curves of devices fabricated with and without 10 wt % PEG-400 on (a) PEDOT:PSS/ITO glass and (b) MoO_3 (10 nm)/ITO glass substrates.

dx.doi.org/10.1021/jp211089n |J. Phys. Chem. C 2012, 116, 1354–1360

polymer probably dissolved in the water.[35] In contrast, the polymer film deposited on the MoO_3 surface had been shed, turning into many small pieces after treatment in the water bath (Figure 6b). We infer that the distribution of PEG was rather uniform in the bulk of the P3HT:PCBM blend; after the dissolution of the PEG polymer, water molecules readily diffused into the polymer film, thereby separating it from the substrate. Figure S2 (Supporting Information) presents the behavior of a more complete set of samples. In short, the water-bath experiments provided direct evidence for the surface energy of the substrates significantly affecting the distribution of the PEG polymer in the blends.[46]

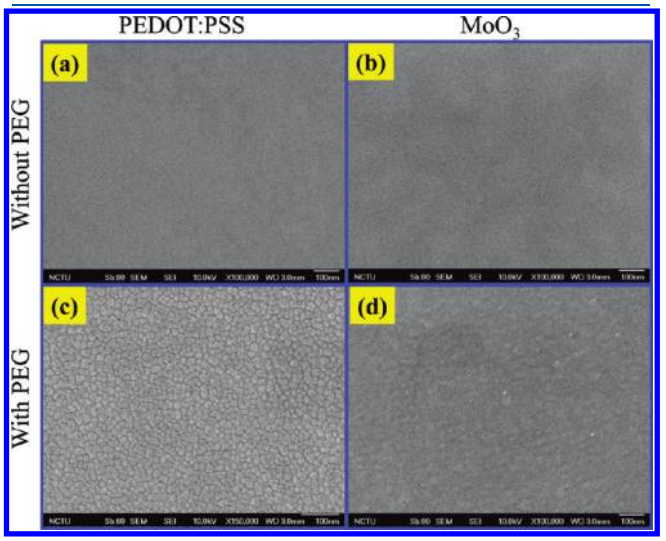

Figure 5. SEM images of P3HT:PCBM thin films prepared (a, b) without and (c, d) with PEG-400 on (a, c) PEDOT:PSS/ITO glass and (b, d) MoO_3/ITO glass substrates.

It is interesting to note that vertical phase separation in polymer blends is also generally observed over large areas no mattter how the film is formed.[48] For example, Madsen et al. used the slot-die coating technique to fabricate the photoactive layer for OPVs and found vertical phase separation in their prepared thin films.[48] In other words, this technique reported herein has high potential to be employed using large-area, high-throughput roll-to-roll fabrications of OPVs.

In addition to device efficiency, device stability is another critical issue affecting the realization of commercial polymer solar panels.[43,48−53] Low-work-function metals, such as calcium, are commonly used as cathode BLs to obtain high PCEs. Unfortunately, these metals are naturally unstable and readily react with moisture and oxygen in the atmosphere. Therefore, it is necessary to develop alternative BLs to improve the device stability. In this study, we found that the devices containing PEG polymers exhibited enhanced environmental stability.[35] Figure 7a displays the normalized PCEs, as a function of time, of P3HT:PCBM devices incorporating self-organized PEG BLs; those of devices prepared with Ca/Al and Al cathodes are included for comparison. All of these devices were stored under ambient conditions, with the specific humidity kept at approximately 50%. The test protocols were qualified as an ISOS-D-1 experiment.[54] These tested devices were not encapsulated; that is, the cathodes were exposed directly to the atmosphere. The PCE decreased dramatically for the device fabricated with Ca/Al as the cathode, reaching almost zero (ca. 0.03%) after 22 days, presumably

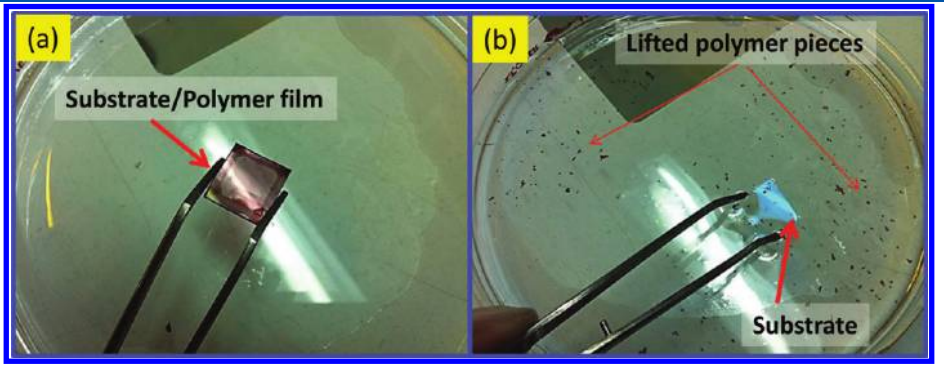

Figure 6. Photographs of P3HT:PCBM:10% PEG-400 samples prepared on (a) PEDOT:PSS/ITO glass and (b) MoO_3/ITO glass after treatment in a water bath.

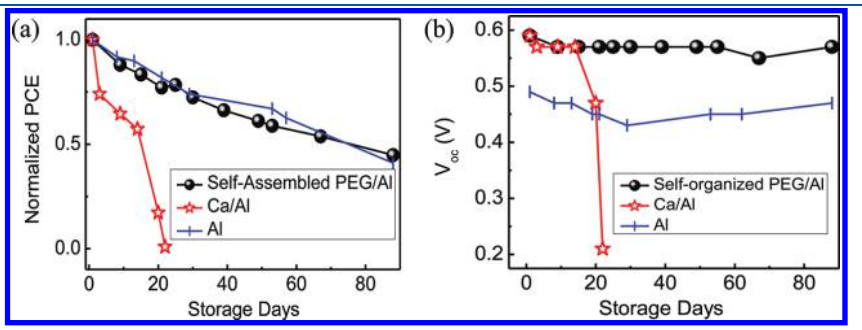

Figure 7. (a) Normalized PCEs and (b) open-circuit voltages (V_{oc}) of devices fabricated with various cathode structures plotted as functions of time. These devices, which were not encapsulated, were stored in a cabinet in which the relative humidity was controlled at ca. 50%.

because of the high reactivity of Ca atoms. In comparison, the device incorporating the self-organized PEG BL exhibited higher stability. Figure 7 b presents the values of V_{oc}, which is directly related to the natural properties of the contact, of these devices. The value of V_{oc} of the Ca-based device degraded rapidly from 0.59 to 0.21 V within 22 days, whereas the photovoltage of the devices incorporating the self-organized PEG BL remained almost unchanged after 90 days, revealing the high stability of the PEG/Al interfaces.

CONCLUSIONS

The presence of self-organized PEG BLs at the cathode contacts can result in high-performance polymer solar cells. After drying of the polymer blend, the additive PEG polymers tend to migrate to the surface of the active layer to achieve thermodynamic equilibrium, thereafter serving as a natural nanoscale BL. The PEG layer effectively modifies the work function of the Al electrode and decreases the contact resistance between the active layer and the metal cathode. This approach requires only a single fabrication step to simultaneously deposit the photoactive layer and the cathode BL. In terms of kinetics, PEG polymers of lower molecular weight undergo more efficient vertical phase separation in the polymer blends than do their high-M_w counterparts, which might not be able to phase separate to the surface prior to solidification of the polymer films due to lower mobilities. We also found that the surface energy of the substrate plays an important role in triggering the formation of the vertical-type morphology. Devices prepared using this approach exhibited stabilities superior to those of traditional devices featuring low-work-function metals as cathode BLs. On the basis of our new understanding of the mechanism behind the vertical phase separation, we fabricated OPVs displaying both high efficiency and appreciable improvement in stability. We foresee that this approach might be of further use in other material systems, such as recently developed low-band-gap polymers, to achieve even higher PCEs and enhanced stability.

ASSOCIATED CONTENT

Supporting Information. SEM images of a P3HT:PCBM polymer film containing 10 wt % PEG-6000, detailed OPV performance (with and without PEG-400) prepared on PEDOT:PSS or MoO_3 surfaces, and photographs of P3HT:PCBM films with and without 10 wt % PEG-400 depositied on PEDOT:PSS and MoO_3 surfaces before and after water bath treatment. This material is available free of charge via the Internet at http://pubs.acs.org.

AUTHOR INFORMATION

Corresponding Author

*E-mail: fcchen@mail.nctu.edu.tw.

ACKNOWLEDGMENT

This study was supported by the National Science Council (Grants NSC 100-3113-E-009-005 and NSC 100-2221-E-009-082) and the Ministry of Education through the ATU Program.

REFERENCES

(1) Panwar, N. L.; Kaushik, S. C.; Kothari, S. *Renewable Sustainable Energy Rev.* **2011**, *15*, 1513–1524.
(2) Baxter, J.; Bian, Z. X.; Chen, G.; Danielson, D.; Dresselhaus, M. S.; Fedorov, A. G.; Fisher, T. S.; Jones, C. W.; Maginn, E.; Kortshagen, U.; Manthiram, A.; Nozik, A.; Rolison, D. R.; Sands, T.; Shi, L.; Sholl, D.; Wu, Y. Y. *Energy Environ. Sci.* **2009**, *2*, 559–588.
(3) Liang, Y. Y.; Xu, Z.; Xia, J. B.; Tsai, S. T.; Wu, Y.; Li, G.; Ray, C.; Yu, L. P. *Adv. Mater.* **2010**, *22*, E135–E138.
(4) Dennler, G.; Scharber, M. C.; Brabec, C. J. *Adv. Mater.* **2009**, *21*, 1323–1338.
(5) Mayer, A. C.; Scully, S. R.; Hardin, B. E.; Rowell, M. W.; McGehee, M. D. *Mater. Today* **2007**, *10*, 28–33.
(6) Arias, A. C.; MacKenzie, J. D.; McCulloch, I.; Rivnay, J.; Salleo, A. *Chem. Rev.* **2010**, *110*, 3–24.
(7) Lipomi, D. J.; Tee, B. C. K.; Vosgueritchian, M.; Bao, Z. N. *Adv. Mater.* **2011**, *23*, 1771–1775.
(8) Krebs, F. C.; Tromholt, T.; Jorgensen, M. *Nanoscale* **2010**, *2*, 873–886.
(9) Garcia-Valverde, R.; Cherni, J. A.; Urbina, A. *Prog. Photovoltaics* **2010**, *18*, 535–558.
(10) Espinosa, N.; Garcia-Valverde, R.; Urbina, A.; Krebs, F. C. *Sol. Energy Mater. Sol. Cells* **2011**, *95*, 1293–1302.
(11) Veldman, D.; Meskers, S. C. J.; Janssen, R. A. *Adv. Funct. Mater.* **2009**, *19*, 1939–1948.
(12) Morteani, A. C.; Sreearunothai, P.; Herz, L. M.; Friend, R. H.; Silva, C. *Phys. Rev. Lett.* **2004**, *92*, 247402.
(13) Yu, G.; Gao, J.; Hummelen, J. C.; Wudl, F.; Heeger, A. J. *Science* **1995**, *270*, 1789–1791.
(14) Li, G.; Shrotriya, V.; Huang, J.; Yao, Y.; Moriarty, T.; Emery, K.; Yang, Y. *Nat. Mater.* **2005**, *4*, 864–868.
(15) Ko, C. J.; Lin, Y. K.; Chen, F. C. *Adv. Mater.* **2007**, *19*, -3520–3523.
(16) Bulliard, X.; Ihn, S.-G.; Yun, S.; Kim, Y.; Choi, D.; Choi, J.-Y.; Kim, M.; Sim, M.; Park, J.-H.; Choi, W.; Cho, K. *Adv. Funct. Mater.* **2010**, *20*, 4381–4387.
(17) Chen, F. C.; Tseng, H. C.; Ko, C. J. *Appl. Phys. Lett.* **2008**, *92*, 023307.
(18) Chen, H. Y.; Hou, J. H.; Zhang, S. Q.; Liang, Y. Y.; Yang, G. W.; Yang, Y.; Yu, L. P.; Wu, Y.; Li, G. *Nat. Photonics* **2009**, *3*, 649–653.
(19) Sun, Y.; Seo., J. H.; Takacs, C. J.; Seifter, J.; Heeger, A. J. *Adv. Mater.* **2011**, 1679–1683.
(20) Zhao, G.; He, Y.; Li, Y. *Adv. Mater.* **2010**, *22*, 4355–4358.
(21) Chen, Y. C.; Yu, C. Y.; Lin, Y. L.; Fan, L.; Hung, I.; Chen, C. P.; Ting, C. *Chem. Commun.* **2010**, *46*, 6503–6505.
(22) Norrman, K.; Madsen, M. V.; Gevorgyan, S. A.; Krebs, F. C. *J. Am. Chem. Soc.* **2010**, *132*, 16883–16892.
(23) Po, R.; Carbonera, C.; Bernardi, A.; Camaioni, N. *Energy Environ. Sci.* **2011**, *4*, 285–310.
(24) Ma, H.; Yip, H.-L.; Huang, F.; Jen, A. K. Y. *Adv. Funct. Mater.* **2010**, *20*, 1371–1388.
(25) Brabec, C. J.; Cravino, A.; Meissner, D.; Sariciftci, N. S.; Fromherz, T.; Rispens, M. T.; Sanchez, L; Hummelen, J. C. *Adv. Funct. Mater.* **2001**, *11*, 374–380.
(26) Gomez, E. D.; Loo, Y.-L. *J. Mater. Chem.* **2010**, *20*, 6604–6611.
(27) Li, S. S.; Tu, K. H.; Lin, C. C.; Chen, C. W.; Chhowalla, M. *ACS Nano* **2010**, *4*, 3169–3174.
(28) Cook, R. M.; Pegg, L. J.; Kinnear, S. L.; Hutter, O. S.; Morris, R. J. H.; Hatton, R. A. *Adv. Energy Mater.* **2011**, *1*, 440–447.
(29) Brabec, C. J.; Shaheen, S. E.; Winder, C.; Sariciftci, N. S.; Denk, P. *Appl. Phys. Lett.* **2002**, *80*, 1288.
(30) Jiang, X.; Xu, H.; Yang, L.; Shi, M.; Wang, M.; Chen, H. *Sol. Energy Mater. Sol. Cells* **2009**, *93*, 650–653.
(31) Chen, F.-C.; Wu, J.-L.; Yang, S. S.; Hsieh, K.-H.; Chen, W.-C. *J. Appl. Phys.* **2008**, *103*, 103721.
(32) Oh, S.-H.; Na, S.-I.; Jo, J.; Lim, B.; Vak, D.; Kim, D.-Y. *Adv. Funct. Mater.* **2010**, *20*, 1977–1983.
(33) Zhang, F.; Ceder, M.; Inganäs, O. *Adv. Mater.* **2007**, *19*, 1835–1838.
(34) Debettignies, R.; Leroy, J.; Firon, M.; Sentein, C. *Synth. Met.* **2006**, *156*, 510–513.

(35) Chen, F.-C.; Chien, S.-C. *J. Mater. Chem.* **2009**, *19*, 6865–6869.
(36) Lee, T.-H.; Huang, J.-C.-A.; Pakhomov, G. L. V.; Guo, T.-F.; Wen, T.-C.; Huang, Y.-S.; Tsou, C.-C.; Chung, C.-T.; Lin, Y.-C.; Hsu, Y.-J. *Adv. Funct. Mater.* **2008**, *18*, 3036–3042.
(37) Tai, Q. D.; Li, J. H.; Liu, Z. K.; Sun, Z. H.; Zhao, X. Z.; Yan, F. *J. Mater. Chem.* **2011**, *21*, 6848–6853.
(38) Jung, J. W.; Jo, J. W.; Jo, W. H. *Adv. Mater.* **2011**, *23*, 6.
(39) Chen, F. C.; Ko, C. J.; Wu, J.-L.; Chen, W. C. *Sol. Energy Mater. Sol. Cells* **2010**, *94*, 2426–2430.
(40) Shrotriya, V.; Li, G.; Yao, Y.; Moriarty, T.; Emery, K.; Yang, Y. *Adv. Funct. Mater.* **2006**, *16*, 2016–2023.
(41) Kuo, C.-H.; Chang, H.-Y.; Liu, C.-P.; Lee, S.-H.; You, Y.-W.; Shyue, J.-J. *Phys. Chem. Chem. Phys.* **2011**, *13*, 3649–3653.
(42) Sun, Y.; Wang, M.; Gong, X.; Seo, J. H.; Hsu, B. B. Y.; Wudl, F.; Heeger, A. J. *J. Mater. Chem.* **2011**, *21*, 1365–1367.
(43) Kumar, A.; Rosen, N.; Devine, R.; Yang, Y. *Energy Environ. Sci* **2011**, *4*, 4917–4920.
(44) Chen, F.-C.; Lin, Y.-K.; Ko, C.-J. *Appl. Phys. Lett.* **2008**, *92*, 023307.
(45) Bjorstrom, C.; Nilsson, S.; Bernasik, A.; Budkowski, A.; Andersson, M.; Magnusson, K.; Moons, E. *Appl. Surf. Sci.* **2007**, *253*, 3906–3912.
(46) Chen, F.-C.; Chuang, M.-K.; Chien, S.-C.; Fang, J.-H.; Chu, C.-W. *J. Mater. Chem.* **2011**, *21*, 11378–11382.
(47) Fox, H. W.; Zisman, W. A. *J. Colloid Sci.* **1950**, *5*, 514–531.
(48) Madsen, M. V.; Sylvester-Hvid, K. O.; Dastmalchi, B.; Hingerl, K.; Norrman, K.; Tromholt,; Manceau, M.; Angmo, D.; Krebs, F. C. *J. Phys. Chem. C* **2011**, *115*, 10817–10822.
(49) Hsieh, C. H.; Cheng, Y. J.; Li., P. J.; Chen, C. H.; Dubosc, M.; Liang, R. M.; Hsu, C. S. *J. Am. Chem. Soc.* **2010**, *132*, 4887–4893.
(50) Gao, D.; Helander, M. G.; Wang, Z. B.; Puzzo, D. P.; Greiner, M. T.; Lu, Z. H. *Adv. Mater.* **2010**, *22*, 5404–5408.
(51) Kumar, A., Z.; Hong, R.; Sista, S.; Yang, Y. *Adv. Energy Mater* **2011**, *1*, 124–131.
(52) Gevorgyan, S. A.; Medford, A. J.; Bundgaard, E.; Sapkota, S. B.; Schleiermacher, H.; Zimmermann, B.; Würfel, U.; Chafiq, A.; Lira-Cantu, M.; Swonke, T.; Wagner, M.; Brabec, C. J.; Haillant, O.; Voroshazi, E.; Aernouts, T.; Steim, R.; Hauch, J. A.; Elschner, A.; Pannone, M.; Xiao, M.; Langzettel, A.; Laird, D.; Lloyd, M. T.; Rath, T.; Maier, E.; Trimmel, G.; Hermenau, M.; Menke, T.; Leo, K.; Rösch, R.; Seeland, M.; Hoppe, H.; Nagle, T. J.; Burke, K. B.; Fell, C. J.; Vak, D.; Singh, T. B.; Watkins, S. E.; Galagan, Y.; Manor, A.; Katz, E. A.; Kim, T.; Kim, K.; Sommeling, P. M.; Verhees, W. J. H.; Veenstra, S. C.; Riede, M.; Christoforo, G. M.; Currier, T.; Shrotriya, V.; Schwartz, G.; Krebs, F. C. *Sol. Energy Mater. Sol. Cells* **2011**, *95*, 1398–1416.
(53) Jorgensen, M.; Norrman, K.; Krebs, F. C. *Sol. Energy Mater. Sol. Cells* **2008**, *92*, 686–714.
(54) Reese, M. O.; Gevorgyan, S. A.; Jørgensen, M.; Bundgaard, E.; Kurtz, S. R.; Ginley, D. S.; Olson, D. C.; Lloyd, M. T.; Morvillo, P.; Katz, E. A.; Elschner, A.; Haillant, O.; Currier, T. R.; Shrotriya, V.; Hermenau, M.; Riede, M.; Kirov, K. R.; Trimmel, G.; Rath, T.; Inganas, O.; Zhang, F.; Andersson, M.; Tvingstedt, K.; Lira-Cantu, M.; Laird, D.; McGuiness, C.; Gowrisanker, S. (J.); Pannone, M.; Xiao, M.; Hauch, J.; Steim, R.; DeLongchamp, D. M.; Rösch, R.; Hoppe, H.; Espinosa, N.; Urbina, A.; Yaman-Uzunoglu, G.; Bonekamp, J.-B.; van Breemen, A. J. J. M.; Girotto, C.; Voroshazi, E.; Krebs, F. C. *Sol. Energy Mater. Sol. Cells* **2011**, *95*, 1253–1267.